SAND2020-13263C

Vertical-Axis Wind Turbine Steady and Unsteady Aerodynamics for Curved Deforming Blades

Kevin R. Moore* and Brandon L. Ennis†
Sandia National Laboratories‡, Albuquerque, NM 87185

With interest resurging in vertical-axis wind turbines, there is a need for a fast and accurate vertical-axis turbine aerodynamics model. Although 3-D vortex methods are faster than 3-D computational fluid dynamics, they are orders of magnitude slower than required for design optimization. Lower fidelity models like actuator cylinder and double multiple streamtube are popular choices. However, both original formulations assume a steady-state infinite cylinder of unchanging radius, uncharacteristic of offshore turbines. Although stacks of cylinders can be used to approximate curved blades, this yields errors in excess of 50% and does not capture active deformation. Despite current consensus that these are errors inherent to the 2-D formulation, we show the error can nearly all be resolved by including considerations for curved blades. Unsteady effects have historically been captured using a first-order filter on the steady-state induced velocities. Although active deformation can be captured with proper discretization, the unsteady model requires a full revolution solution at each timestep. We found that with a rotating point iterative approach, only solutions at the blade positions are required, which gives a 5-10x speedup. These modifications together enable full-turbine unsteady simulations with accuracy comparable to vortex methods, but as much as 5000x faster.

I. Introduction

VERTICAL axis wind turbine (VAWT) aerodynamics are unique in that the blades pass through their own wake capturing energy and inducing velocity in both the upstream and downstream areas (as depicted in Fig. 1). This requires the mutual influence of the upwind and downwind portions to be calculated for accurate predictions. Although vortex methods and computational fluid dynamics (CFD) do this very well, a faster method is needed to enable trade studies, fully coupled aerostructural analysis, and optimization. The need for a simplified aerodynamics model has led to many variations including streamtube [1], multiple streamtube [2, 3], double multiple streamtube (DMS) [4–6], and actuator cylinder (AC) theory [7]. DMS and AC are the primary models used, with AC being more preferred [8–10] due to its more physically accurate nature [11]. However, DMS is generally comparable and runs approximately 20x faster.

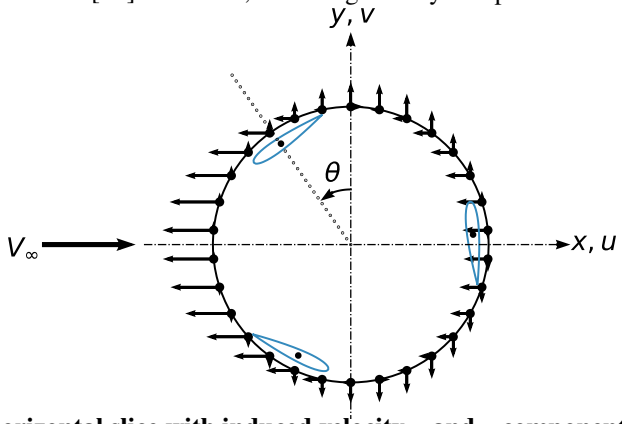

Fig. 1 VAWT 2-D horizontal slice with induced velocity u and v components depicted by arrows.

*Senior Member of the Technical Staff, Wind Energy Technologies, PO Box 5800, MS 1124, Member AIAA.
†Senior Member of the Technical Staff, Wind Energy Technologies, PO Box 5800 MS 1124.
‡Sandia National Laboratories is a multimission laboratory managed and operated by National Technology and Engineering Solutions of Sandia, LLC., a wholly owned subsidiary of Honeywell International, Inc., for the U.S. Department of Energy's National Nuclear Security Administration under contract DE-NA-0003525

Both the DMS and AC formulations were originally derived for a steady-state infinite cylinder of unchanging radius. Although these simplifications have been proven useful, they are not representative of a large VAWT with curved deforming blades. Previous studies have shown that stacks of cylinders can be used to approximate 3-D curved blades [8, 12] however, a rigorous validation of this approximation has not been made. This is partly due to the general lack of the appropriate aerodynamic data for vertical-axis wind turbines. For example, the Sandia 17 meter turbine has aerodynamic data at the center of the turbine where the blade is vertical but not at the curved areas [13]. Additionally, the Sandia 34 meter, though highly instrumented, did not include blade pressure distribution instrumentation [14]. In this paper, we use the Sandia 5 meter turbine [15]. We first validate a 3-D vortex method, CACTUS [16], using turbine performance data, then use the vortex method's detailed loads as pseudo-validation data for AC and DMS.

In a recent paper by Tavernier [17], many fully 3-D and pseudo 3-D VAWT models are compared. The authors identify CACTUS as the most physically accurate and show the stacked AC method as the most similar, but with significant differences in predicted loads for highly sloped blade regions. Other studies that attempt to add blade slope considerations for either AC or DMS [9, 12, 18–20] are focused on other objectives, are inconsistent in how the modifications are made, and lack blade-element level verification. Only Leroy [20] seems to fully address blade slope, but it is done in passing for only DMS and without blade-element level verification. The general consensus seems to be that the differences in predicted loads between these 2-D and 3-D models is inherent to 2-D limitations. However, by revisiting the fundamental assumptions in a curved-blade frame of reference, the 2-D models can account for the majority of what were previously described as 3-D effects. Additionally, details for handling actively deforming blades are limited in the literature and are revisited in this study. Finally, we also revisit the method that makes these steady models operate in the unsteady domain and identify a numerically superior solution method.

II. Baseline Model Theory

A. Actuator Cylinder and Double Multiple Streamtube

Both the AC and DMS methods have no closed form solution, but rather require an iterative solution similar to blade element momentum theory [21]. These models solve for the aerodynamic flow field subject to blade forces, while the blade forces depend on the flow field. The methods both use a residual equation to solve for the turbine induced velocities which are iterated on until the blade-induced velocities equal the input velocities. The blade element forces are calculated similarly for both methods using the normal and tangential velocities due to freestream, blade motion, and induction. Both methods also use the stacked disk method to approximate a 3-D turbine, and each disk is completely independent. Any improvements gained by revisiting the models from a curved and deforming frame of reference can be applied to the blade element portions of both methods.

Our specific AC implementation is based on Ning's work [12] due it its full definition of frames of reference, equations, and availability of open source code. Our DMS implementation is based on Ayati's work [6] due to similar levels of detail in equations.

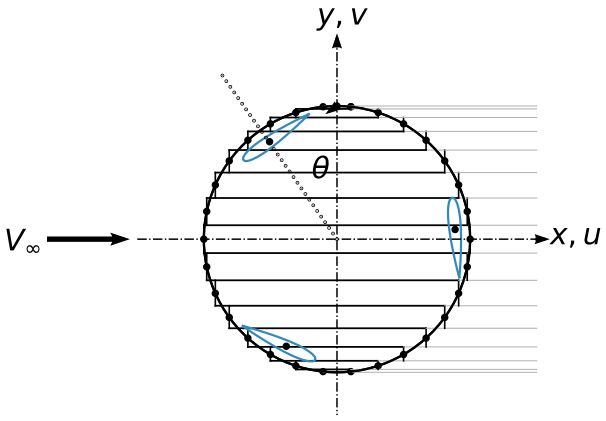

Fig. 2 Depiction of DMS streamtubes of constant angular discretization. Aerodynamic coupling one-way with respect to the downstream (light grey tubes) using the upstream (black tubes) exit velocity for a given streamtube.

The AC and DMS methods differ in how adjacent locations around the cylinder affect one another. For DMS, the only coupling is between two collinear streamtubes where the outlet velocity of the upstream is imposed as the inlet condition on the downstream (see Fig. 2). Because of the simple nature of the coupling, the only assumption required is that respective upstream and downstream streamtubes remain relatively aligned. Because of the intuitive and straightforward nature of shifting the index between upstream and downstream streamtubes so the coupling is realigned with the freestream, we do not explore it. However, the intra-turbine coupling in AC is much less straightforward. All azimuthal locations affect one another with what has been termed as an *influence coefficient* matrix [12]. This matrix is the influence factor of every position on every other position, but was also originally derived for an unchanging radius and straight blades.

B. Unsteady Approximation

The method to approximate unsteady characteristics for a VAWT using AC or DMS has historically been a first order time filter [22]. This is similar to the method used for horizontal-axis wind turbine (HAWT) blade element momentum theory [23] and has been used in the VAWT adaptations of HAWC2 [8, 22], SIMO-RIFLEX-AC [9], and a TU Delft study [10].

The first order filter method is a three step process incorporating what we will term as near and far wake influences. First, AC or DMS is solved for steady-state using the current conditions (near wake influence). Second, the resulting induced velocities are combined with historical induced velocities (far wake) using the filter. Third, the filtered induced velocities are then used to get the turbine performance at the current timestep. This process is repeated at each timestep for all time. Details on the specific equations can be found in [22].

III. Steady-State Theory Modifications

A. Baseline Turbine for Verification

Prior to introducing modifications to the models, we define a baseline turbine and model setup that will be used for verifying the modifications. We use the Sandia National Laboratories (SNL) three-bladed 5 meter turbine [24], upgraded with full troposkein NACA-0015 blades [15]. This turbine was chosen for its simplicity and availability of performance data. The turbine is 5 meters in diameter, has a height to diameter ratio of 1.02, a constant chord of 6 inches, and zero degrees installed twist, but a 40% chord mount point (which gives an effective twist that varies along the blade, see [25]). We model the SNL 5m with CACTUS, AC, and DMS using 31 vertical discretizations (making 30 slices). The CACTUS case models the turbine in full 3-D, while the AC and DMS cases use the stacked cylinder approach. All cases use the Boeing-Vertol [26] dynamic stall model and 30 timesteps per revolutions unless otherwise specified. The flow conditions are matched with the nominal test site parameters (Albuquerque, NM). The rotor rotation rate was held constant at 150 RPM. The curvature, local radius, and other required parameters are based on the nominal turbine parameters and troposkein shape. Figure 3 shows the turbine and the troposkein shape. For CACTUS specifically, the wake cutoff parameter was set at 3 diameters, and the model was run until the change in coefficient of performance had converged below 1E-4 unless otherwise specified.

Fig. 3 SNL 5m three-bladed turbine showing troposkein shape.

B. Blade Element Theory Modifications

As stated previously, the original formulations for DMS and AC assumed an infinite cylinder (straight blades). This assumption was also used in the blade element formulations. Even though the original model derivations use the term *normal*, they do not include cases where the normal vector differs from the radial vector. Solving for curved blades with only the radial component does not yield the same solution as solving with the true normal. Additionally, this effect cannot be captured by simply stacking an infinite number of cylinders in the same way that the diagonal distance between two points cannot be approximated by an infinite number of zig-zags. The slope must be included.

Blade slope is defined from the vertical-axis by the arctangent of the change in x-direction divided by the change in z-direction. Therefore, blade slope is positive for the lower portions of the blade and negative for the upper. This follows right hand rule convention when aligned with the blade tangential direction of motion. The angle from the horizontal axis to the blade normal equals the blade slope angle because the blade slope and blade normal are perpendicular. To convert from the radial to normal frame of reference is a simple trigonometric matter. However, as depicted in Fig. 4, blade slope affects forces and velocities differently.

The frame of reference used in this paper is consistent with Ning [12]. Of note is that positive velocities are in the following directions: vertical is towards the top of the turbine, radial is towards the center of rotation, and tangential is towards the blade leading edge (opposite of the advancing blade direction). Positive forces are in the opposite direction; they are the forces the blades exert on the fluid. More details and depictions can be found in Ning's paper.

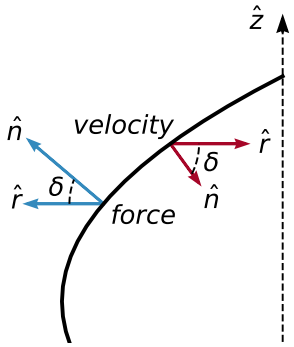

Fig. 4 Force and velocity vectors transformed from radial to normal.

1. Blade Slope Effects on Velocity

Local normal and tangential velocities are used to calculate the local blade angle of attack and local velocity magnitude, both of which have a strong influence on the local blade forces. For the 2-D models, the normal velocity V_n is calculated via the blade slope δ and azimuthal angle θ from the local radial velocity due to the freestream V_∞ and induced velocity flow field u and v. This is shown in the left side of Eq. (1). The tangential velocity needs no correction as it is perpendicular to changes in blade slope. While Wang [19] does show blade slope considerations in his velocity equations, he does not completely include blade slope effects on forces. Only Leroy [20] seems to fully address blade slope, but it is done in passing for only DMS without any blade-element level verification. The right hand portions of Eq. (1) show how velocities from deformation can be added.

$$\begin{aligned} V_n &= \overbrace{\left(V_\infty(1+u)\sin\theta - V_\infty(v)\cos\theta\right) * \cos\delta}^{\text{from freestream, induction, rotation}} \quad \overbrace{+ V_{\text{vertical}} * \sin\delta + V_{\text{radial}} * \cos\delta}^{\text{from deformations}} \\ V_t &= V_\infty(1+u)\cos\theta + V_\infty(v)\sin\theta + \Omega r \qquad + V_{\text{tangential}} \end{aligned} \tag{1}$$

2. Blade Slope Effects on Force

Blade slope has two effects on forces: first, element span length, and second, how normal force is resolved into radial and vertical force. In the blade element formulations used by DMS and AC, once the local velocity vector is known, the local airfoil 2-D lift and drag coefficients can be found from airfoil polars. These coefficients are then rotated by the local inflow direction to get the local blade normal and tangential force coefficients c_n and c_t. However, the airfoil 2-D lift and drag coefficients used are per unit span. For a turbine slice of unit height, the sloped blades' span is not the same as the unit height, but is increased by dividing by the cosine of the blade slope. The modification required for the discrete normal force F'_{n} used in the AC residual equation is shown in Eq. (2) (compare Ning [12] Eq. 28 and note that radial loading should now be termed normal loading). The modification for the DMS thrust force T'_h used in its residual equation is shown in Eq. (3) (compare Ayati [6] Eq. 11). Air density is ρ, local velocity magnitude is W, chord length is c, and B is number of blades. Both equations assume unit height. Although this modification was discussed in part by Cheng [18], no mention was made of the other modifications needed and only high level validation was done.

$$F'_{\text{n}} = \frac{c_{\text{n}}}{\cos\delta}\frac{1}{2}\rho W^2 c\frac{B\Delta\theta}{2\pi} \tag{2}$$

$$T'_h = \frac{1}{2}\rho W^2 c\frac{(c_t\cos\theta + c_n\sin\theta)}{\cos\delta} \tag{3}$$

More intuitively, blade slope allows us to break a normal vector into radial and vertical components. The normal force is multiplied by the cosine of δ to get radial and multiplied by the sin of δ to get vertical. However, the aforementioned

span length must also be included. The resulting reduced equations are shown in Eq. (4) and match those given by Ning [12] including the frame of reference. Ning discusses these effects for output forces in full detail, but does not include the slope in the residual or velocity equations. F'_R, F'_T, and F'_Z are the radial, tangential, and vertical force per unit height.

$$\begin{aligned} F'_R &= -c_n \frac{1}{2}\rho W^2 c \\ F'_T &= c_t \frac{1}{2}\rho W^2 \frac{c}{\cos\delta} \\ F'_Z &= -c_n \frac{1}{2}\rho W^2 c \tan\delta \end{aligned} \tag{4}$$

Also of note is that the AC instantaneous thrust F'_X used for the AC nonlinear correction factor is the force parallel to the freestream. This force is comprised of the radial and tangential forces as shown in Eq. (5) and is also correctly defined by Ning for curved blades (compare Ning [12] Eq. 35).

$$F'_X = -F'_R \sin\theta - F'_T \cos\theta \tag{5}$$

3. Verification

The effects of the blade slope corrections as previously described are shown in Fig. 5. The case shown is of the baseline Sandia 5 meter turbine for a tip speed ratio (TSR) of 5.2. The AC and DMS models were run using stair-stepped vertical slices (piecewise straight blades) and the improved formulation including slope just described. The AC and DMS models are compared in the figure with CACTUS results for the average tangential force along the vertical axis, using CACTUS as the "truth" model. This measure was chosen to give a 3-D projection of the high level accuracy of the models' blade load predictions, particularly concerning turbine torque performance. Similar effects are seen for the full range of TSR and for the other forces. The curved models match much better than the straight over the entire height of the turbine. Surprisingly, (as will be shown in the steady-state validation section) the curved models' vertical forces are in such good agreement with CACTUS, that the vertical induction for this type of turbine may not be as significant as previously thought.

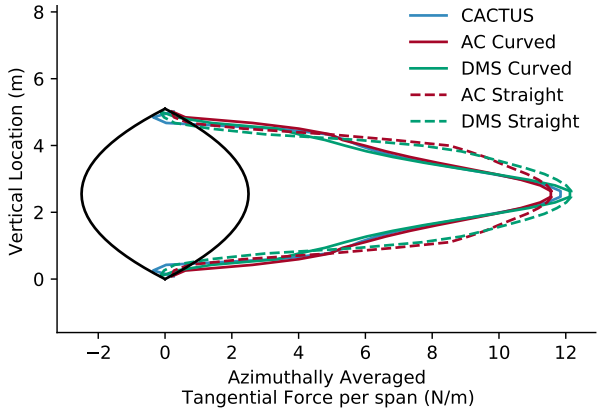

Fig. 5 Average tangential force per span along vertical-axis for SNL 5 meter turbine at TSR of 5.2. Turbine blade shape is in black. Blade slope considerations decrease error compared with the CACTUS 3-D vortex method.

C. Actuator Cylinder Intra-Turbine Coupling

The actuator cylinder method commonly used today is actually a linearized version with a nonlinear correction term. By linearizing the method, significant computational improvements can be made. However, even greater improvements can be made by reducing the computation required for the intra-turbine influence coefficients. The original formulation did this by assuming an unchanging unit radius and no blade slope. By doing this, the relatively expensive computation

associated with integrating each influence term can be done once and reused for any turbine or operating condition. The matrix becomes only dependent on the azimuthal discretization. While a curved deforming blade violates the assumptions stated above, we will show that under most conditions this original formulation may be used with minimal error.

To determine what the influence coefficient matrix should be for a curved deforming blade, we re-derive the linearized equations in 3-D. This is done by starting with the nonlinear actuator surface method [27] and linearizing it using the process for the 2-D AC method as described in Appendix A of Cheng's paper [18]. Including the normal force and velocity considerations in 3-D during this process results in the pressure equation shown in Eq. (6).

$$p = \int_0^h \int_0^{2\pi} Q_n \left(r\cos\delta \frac{(-\sin\theta\cos\delta)(x + r\sin\theta) + (\cos\theta\cos\delta)(y - r\cos\theta) + (\sin\delta)(z - z_f)}{\left((x + r\sin\theta)^2 + (y - r\cos\theta)^2 + (z - z_f)^2\right)^{\frac{3}{2}}} \right) d\theta dz \tag{6}$$

The intra-turbine influence portion of the equation is in parenthesis. Although we did complete the derivation for the tangential portion, we do not show it because it is not required for an accurate solution as described by Ning [12] and Cheng [18]. Integrating the equation over the turbine surface for each surface position's influence on each other surface position gives the influence coefficient matrix. The position for which the calculation is being performed is x, y, z and the position where the force is generated is depicted by $r\sin\theta$, $r\cos\theta$, and z_f. The actuator cylinder normal volume force Q_n is as described by Cheng and others (corrected for blade slope as described previously). As a verification, if one assumes a unit radius, no blade slope, and unit height (2-D) then all of the r, $\cos(\delta)$ and z terms drop out. The $\frac{3}{2}$ bottom exponent drops out as well because integration by parts is now done for 2 dimensions instead of 3. The equation then becomes the original infinite-cylinder and unchanging radius equation as described in the literature.

For our purposes, we need to transition this 3-D equation to 2-D. This is done by dropping the z terms and the bottom exponent as described above, but keeping the blade slope and radius terms. However, to maintain the original unit-radius frame of reference, we use a radius vector normalized by the mean section radius. In other words, for a deforming turbine, we use a vector of radii that have all been divided by the mean radius so that the mean now becomes 1. The downside of doing this is that though the influence coefficient matrix is still independent of absolute radius, it must be recalculated every time there is a change in the normalized radius vector or blade slope.

Vectors of parameters/conditions associated with each azimuthally discrete point around the turbine must be used as opposed to singular values. This is how varying blade shape, inflow conditions, rotational speed, and the other varying parameters are incorporated for both the blade element equations and this influence coefficient matrix.

1. Varying Radius

To show the relative effect of varying radius, we define a test case based on a circular path with increasing ovality. This is done using the SNL 5 meter turbine at the constant rotation rate and inflow velocity used previously for the 5.2 TSR case. Additionally we look at a slice at the equator to decouple from blade slope. We keep the mean radius of the oval at the nominal turbine radius, but increase the ovality from 0-100%. Percent ovality is defined as percent elongation of radius along the x-axis, with the y-radius scaled such that the mean radius equals the nominal radius. We then rotate the skewed path from 0 to 180 degrees and find the greatest root mean square error between the two influence coefficient methods to occur with a path tilted approximately 45 degrees. The resulting path is shown in Fig. 6a. We show the solution with the influence coefficient modifications as dashed lines, and the standard approach as straight lines in Fig. 6b. Both types include the varying radius in the blade element equations, but only the modified case has the radius effect in the influence coefficient matrix. Similar levels of difference were seen for the vertical and radial forces. The worst case root mean square error is 0.86 (2.8% of the max absolute value) and occurs with 100% ovality. Error at the peak negative load is 7.7% (approximately 45 degrees azimuth). Error at the peak positive load is 1.5% (approximately 100 degrees azimuth).

Based on this analysis and the minor relative difference, one might neglect the varying radius interaction in the influence coefficient matrix even for a turbine with moderate deformation. One might also neglect this effect during an exploratory phase where the speed associated with a constant influence coefficient matrix is needed. The speed difference of precomputing the influence coefficient matrix can be as much as 7x faster depending on operating conditions, but most cases we ran gave a 2-3x speedup.

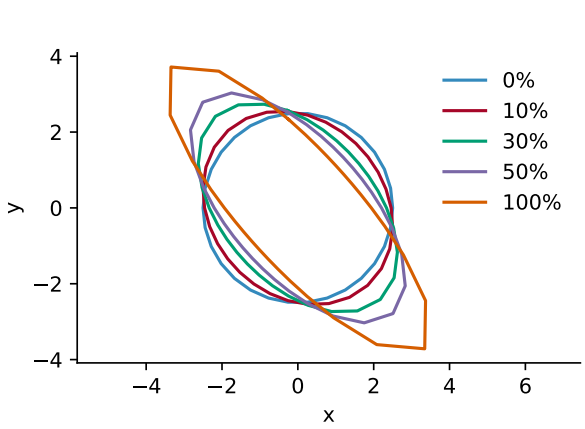

(a) Blade path for varying ovality.

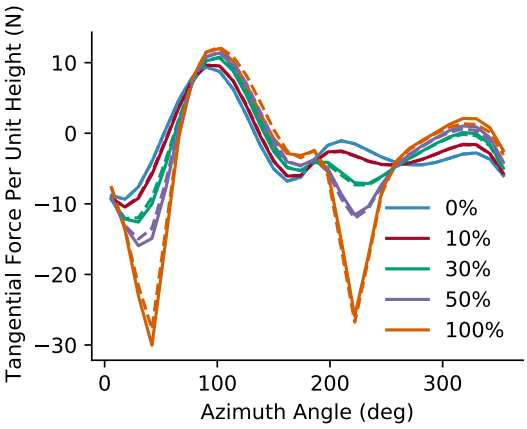

(b) Tangential force for varying ovality. Dahsed lines include influence coefficient modification, straight lines do not.

Fig. 6 Effect of capturing varying radius in the actuator cylinder influence coefficient matrix. Maximum root mean square error is 0.86 for 100% ovality.

2. Varying Blade Slope

To show the relative effect of varying blade slope on the influence coefficients, we use the same SNL 5m turbine at a TSR of 5.2. This turbine naturally has a blade slope ranging from approximately 0-60 degrees. As before, the blade slope vector is included in the blade element equations, but only the modified version includes blade slope in the influence coefficients. Figure 7a shows the resulting revolution-averaged tangential forces and Fig. 7b shows the percent difference. The difference becomes significant as the slope increases towards 60 degrees. However, when we scale the percent difference based on the relative contribution to turbine performance, the difference stays below 1%. This is done by dividing by the corresponding force from Fig. 7a (normalized by the peak force to keep the percent difference frame of reference). Similar levels of difference are seen for the radial and vertical forces. Therefore, similar to a varying radius, it seems that neglecting this effect entirely would be reasonable for this type of turbine. However, turbines with large or actively changing blade slope in areas that contribute significantly to forces would need this modification. This may be the case for a V-VAWT or H-VAWT with tilted blades. Computational speed differences between precomputing or including this effect are the same as for the radius effect and the two modifications should be used together if used.

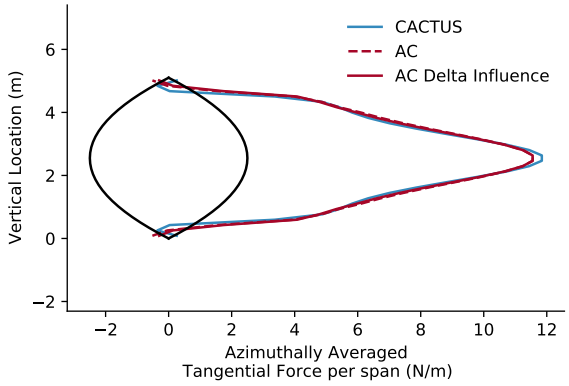

(a) Tangential Force, dashed lines are with radius effects in influence matrix.

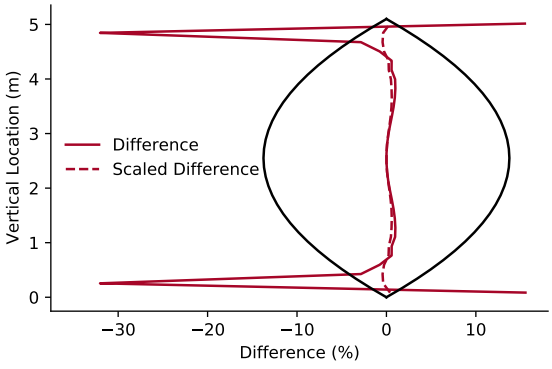

(b) Percent difference where the scaled is the difference multiplied by the normalized span-varying force from Fig. 7a.

Fig. 7 Effect of capturing varying slope in the actuator cylinder influence coefficient matrix. Although the difference becomes significant for increasing slope, the difference as it contributes to the tangential force remains below 1%. Similar differences were seen for the radial and vertical forces.

IV. SNL 5m Steady-State Performance Validation

Prior to exploring unsteady model modifications, it is important to understand that the unsteady model is based on steady-state performance. Therefore, this sections switches from model modifications to fully exercise and validate our implementation of the 2-D steady models. Because there are no recorded azimuthally varying aerodynamic forces for the SNL 5 meter turbine, we first compare against the turbine aggregate performance and then use CACTUS detailed data for a surrogate validation.

Figure 8 shows the turbine coefficient of performance, as measured by experimental torque, versus operational tip speed ratio. The numerical models match well for tip speed ratios between 2 and 4. Above a TSR of 4, there is about a 12% maximum difference between the experiment and simulations. However, all of the numerical models are closely grouped. With the levels of accuracy for the numerical models shown, we move on to the blade level forces.

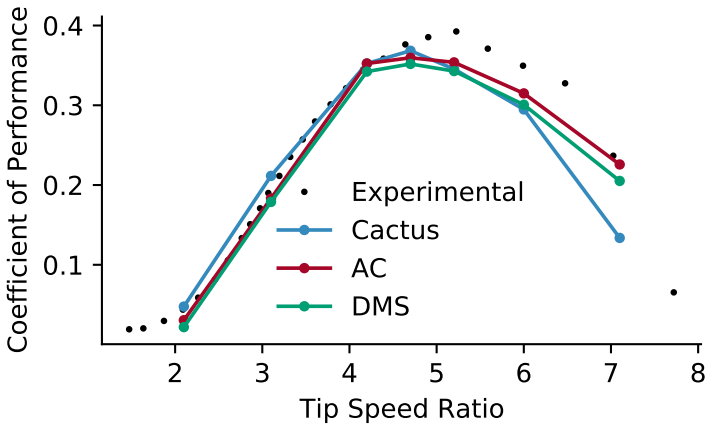

Fig. 8 SNL 5m coefficient of performance comparison with the pseudo 3-D AC and DMS methods.

Figure 9 shows the tangential force of one blade over a revolution at a TSR of 5.2. The two different load profiles correspond to approximately 23% and 49% of the height (slices 7 and 15 of 30). Although the general shape of the load profiles match reasonably well between the higher and lower fidelity models, there is a noticeable deviation in the CACTUS results over the straight airfoil section (49% height). This may be due to 3-D blockage or vertical induction effects increasing inflow towards the center of the turbine. The peak force error for this slice is about 25% and the mean absolute error for either AC or DMS is less than 5% for all slices.

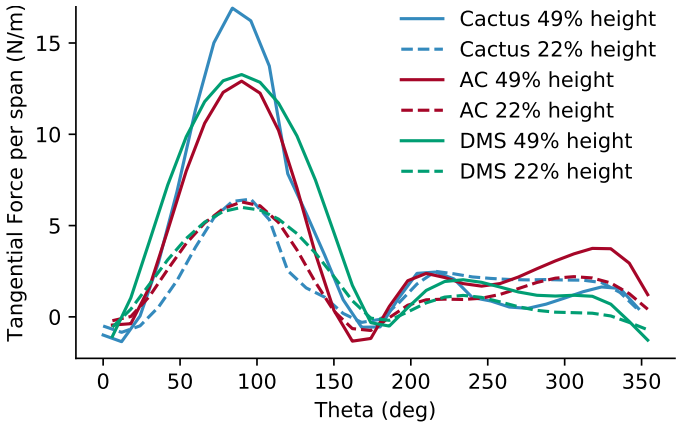

Fig. 9 SNL 5m tangential force comparison between CACTUS, AC, and DMS.

Figure 10 shows both the vertical and radial forces. These forces match better than the tangential with the mean absolute error for both AC and DMS of less than 1% and a peak force error under 15% for radial and 10% for vertical forces. From these high level comparisons, it might be said that the vertical induction for this type of turbine may not be as significant as previously thought.

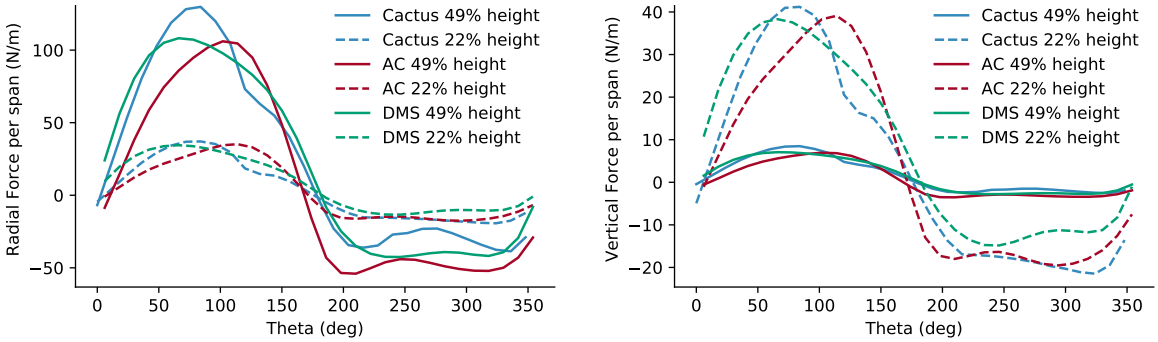

(a) Steady-state radial force.

(b) Steady-state vertical force.

Fig. 10 Radial and vertical force comparisons between CACTUS, AC, and DMS.

V. Unsteady Theory Modifications

As previously described in Section II.B, the current method for unsteady response of the DMS and AC models is via a first order filter on the steady-state induced velocities at each timestep. Because the method is highly dependent on the steady-state solution at each timestep, care must be taken with respect to how the steady formulation is made and how parameters are updated. Otherwise, dynamically changing geometry cannot be accurately captured by these models. Like previously mentioned, the steady-state AC and DMS models' previously singular values, such as radius, inflow velocity, and rotational speed, are made into vectors corresponding with each azimuthal location around the turbine. All of these vectors should be updated at each time step as new information is gained from structures, dynamics, or turbulent inflow, etc. For the majority of parameters, such as rotational speed and radius, this is a simple matter of updating the vectors at the current blade position for a given timestep. In this way, a short history is preserved in the vectors which remains a part of the solution until updated by the next blade that passes. Inflow velocity is the only parameter that must be updated at all positions at each step regardless of blade position.

VAWTs differ from HAWTs in that they have non-negligible depth in the freestream direction. This makes modeling turbulent transport [28] imperative for VAWTs. As a gust passes through the turbine, different sections of the turbine encounter different freestream speeds. A rotating blade can go in and out of the gust as it passes. For example, in Fig. 11 we compare the freestream velocity as seen at the hub versus the freestream velocity seen by blade 1 as it moves up and down stream (blade 1 starts at 0 azimuth angle per Fig. 1). The base simulation used matches the SNL 5 meter 5.2 TSR simulations as previously described. The gust velocity used is a moderate 5 m/s and a duration of 0.8 seconds corresponding to approximately one revolution. This time-changing velocity distribution must be correctly mapped to the numerical vectors corresponding with each azimuthal location for AC and DMS. Additionally, this update must be made for all azimuthal locations at each timestep, regardless of blade position to minimize error.

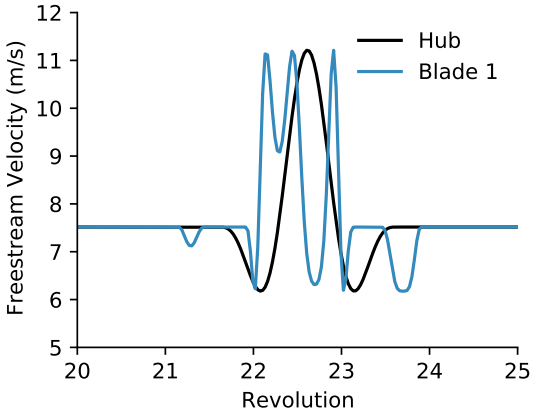

Fig. 11 Freestream velocity at the hub and at blade 1 (as it moves) during large gust passage (at 22% height or slice 7 of 30).

A. Rotating Point Iterative (RPI) Solution Method

The original formulation of the first order filter requires solving for the turbine induced velocity of all blade positions at each timestep. For our discretization, this requires at least 10x more computation than is needed because we are only interested in forces at the blade positions. We found that with careful consideration to how vectors of parameters are updated, the AC or DMS model need only be solved for the blade positions at a given timestep.

Solving AC or DMS for only the blade positions requires what we will term a rotating point iterative (RPI) solution method. This method numerically revolves around the discretized circumference and vectorized parameters following the blade positions. It solves the DMS or AC residual equation with respect to the current blade locations' induced velocities while all other induced velocities and parameters (except incoming freestream velocity as previously discussed) are held constant (see Fig. 1 for a visualization aid). This is done iteratively, shifting the index at each timestep (or as dictated by unsteady dynamics on the rotor position), with the index resetting once the blades begin to overlap the starting points. For a given point along the circumference, this looks like a fixed point iterative method. However, because the index of points being iterated on is rotated, we term it a rotating point iteration. The first order filter is still used to model the unsteady behavior of the turbine, but the original time constants must be retuned (see [22] for more details on these time constants). We found new values of 0.3 and 3.0 for the near and far wake time constants by tuning against CACTUS.

1. RPI Algorithmic Implementation

Algorithm 1 gives an in-depth look at how the RPI method is implemented. For completeness, the algorithm shows how the modifications fit into the first order filter (Line 38). It also shows how to resolve timesteps that cause rotations smaller than the azimuthal discretization as can be common if coupled to unsteady structural dynamics (Line 43). Due to the $O(N^2)$ nature of the AC influence coefficient matrix, using an aerodynamic azimuthal discretization of less than 60 and taking much finer steps may be more computationally effective without sacrificing accuracy. It should also be noted that the algorithm shown assumes Fortran-like one-based indexing.

2. RPI Verification

Using the gust as defined in Fig. 11 and the surrounding text, we compare the AC, DMS and CACTUS models. Note that 36 timesteps per revolution were used. Figure 12 shows the baseline CACTUS response in tangential force for the specified blade position. Referring back to Fig. 11, the gust is centered at revolution 22.75, and has multiple rapid increases and decreases in velocity seen by the passing blade. Looking at Fig. 12 at revolution 20, the loads are periodic steady-state. At revolution 21, there is a slight decrease in the peak force as the blades start to dip into the gust on the upstream, or high torque side. At revolution 22, most of the turbine is in the gust and the high torque side increases and widens. Then, associated with a sharp decrease-increase-decrease in velocity on the downstream, or low torque side, the force spikes just before revolution 23. After revolution 23, the forces tend to return to periodic steady-state. There are several key takeaways here: 1) the 2-D methods capture much of the load profile and variation, but with uniformly lower magnitude peaks than CACTUS (as also seen in Fig. 9). 2) The DMS method gives similar results as AC, favoring the peak upstream loads while under-predicting the secondary downstream loads. 3) The RPI method is nearly identical (less than 1% error) to the 1st order filter method for all cases while being numerically more efficient.

Algorithm 1 Rotating Point Iterative (RPI) Solution Method

Initialize scalars and integers:
Tol # convergence tolerance
N_θ # number of azimuthal discretizations
$\text{step}_{\text{last}}$ # index of last timestep
V_{wakeOld} # average wake velocity at last timestep
B # number of blades
R_{ref} # reference radius
ρ # air density
dt # timestep
$t_{\max}$ # total time
τ_{near} # near wake time constant
τ_{far} # far wake time constant
Initialize arrays and matrices:
ω # rotation rate
r # radius
β # blade twist
δ # blade slope
$V_{\text{inf Local}}$ # local freestream velocity
w_{old} # stacked array of induced velocities for u and v for last timestep
cl, cd $\leftarrow$ getAirfoilPolars
$A \leftarrow$ getInfluenceCoefficients(N_θ) #If DMS, A is not used
for $t \leftarrow 0 : dt : t_{\max}$ **do**
    $w \leftarrow w_{\text{old}}$
    θ, ω_{RPI}, r_{RPI}, β_{RPI}, δ_{RPI}, $V_{\text{inf ALL}}$, $V_{\text{deflections}} \leftarrow$ rotorState (i.e. deformation, dynamics, inflow)
    step $\leftarrow$ ceiling $\left(\frac{\theta}{2\pi/N_\theta}\right)$
    $\text{step}_{\text{circular}} \leftarrow \text{step} - floor\left(\frac{\text{step}-1}{N_\theta B}\right)\frac{N_\theta}{B}$
    $\text{idx}_{\text{RPI}} \leftarrow \left(\text{step}_{\text{circular}}\right) : \left(\frac{N_\theta}{B}\right) : \left(2N_\theta - \frac{N_\theta}{B} + 1 + \text{step}_{\text{circular}}\right)$
    $\omega(\text{idx}_{\text{RPI}}) \leftarrow \omega_{\text{RPI}}$
    $r(\text{idx}_{\text{RPI}}) \leftarrow r_{\text{RPI}}$
    $\beta(\text{idx}_{\text{RPI}}) \leftarrow \beta_{\text{RPI}}$
    $\delta(\text{idx}_{\text{RPI}}) \leftarrow \delta_{\text{RPI}}$
    $V_{\text{inf Local}} \leftarrow V_{\text{inf ALL}}$
    while residual(w, ω, r, β, δ, $V_{\text{inf Local}}$, B, ρ, cl, cd, $V_{\text{deflections}}$, A) > Tol **do**
        $w(\text{idx}_{\text{RPI}}) \leftarrow$ root solver
    end while
    # Get average turbine induction in the freestream direction a
    $[\sim, \sim, \sim, a_{\text{new}}] \leftarrow$ turbinePerformance(w, ω, r, β, δ, $V_{\text{inf Local}}$, B, ρ, cl, cd, $V_{\text{deflections}}$)
    $\tau_1 \leftarrow \tau_{\text{near}} R_{\text{ref}} / V_{\text{wakeOld}}$
    $\tau_2 \leftarrow \tau_{\text{far}} R_{\text{ref}} / V_{\text{wakeOld}}$
    $w_{\text{filtered}} \leftarrow w_{\text{old}} e^{-dt/\tau_1} + w(1 - e^{-dt/\tau_1})$
    $V_{\text{wakeFiltered}} \leftarrow V_{\text{wakeOld}} e^{-dt/\tau_2} + \overline{V_{\text{inf Local}}}(1 - 2a_{\text{new}})(1 - e^{-dt/\tau_2})$ # use average local velocity
    $[R_p(\theta), T_p(\theta), Z_p(\theta), \sim] \leftarrow$ turbinePerformance(w_{filtered}, ω, r, β, δ, $V_{\text{inf Local}}$, B, ρ, cl, cd, $V_{\text{deflections}}$)
    if $\text{step}_{\text{last}} \neq \text{step}$ **then**
        $w_{\text{old}} \leftarrow w_{\text{filtered}}$
        $V_{\text{wakeOld}} \leftarrow V_{\text{wakeFiltered}}$
        $\text{step}_{\text{last}} \leftarrow step$
    end if
end for

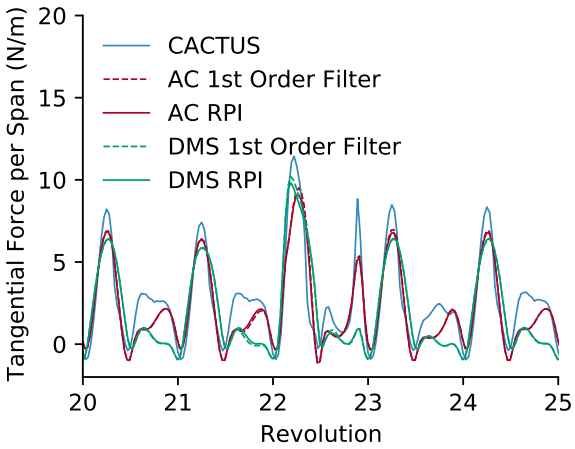

Fig. 12 Tangential force for blade 1 at 22% height (slice 7 of 30). RPI and original 1st order filter methods differ by less than 1%.

The trends for the radial and vertical forces are similar to the tangential force as seen in Fig. 13. Though not shown, these similar trends also are exhibited for the other two blades and as blade slope increases towards the top of the turbine.

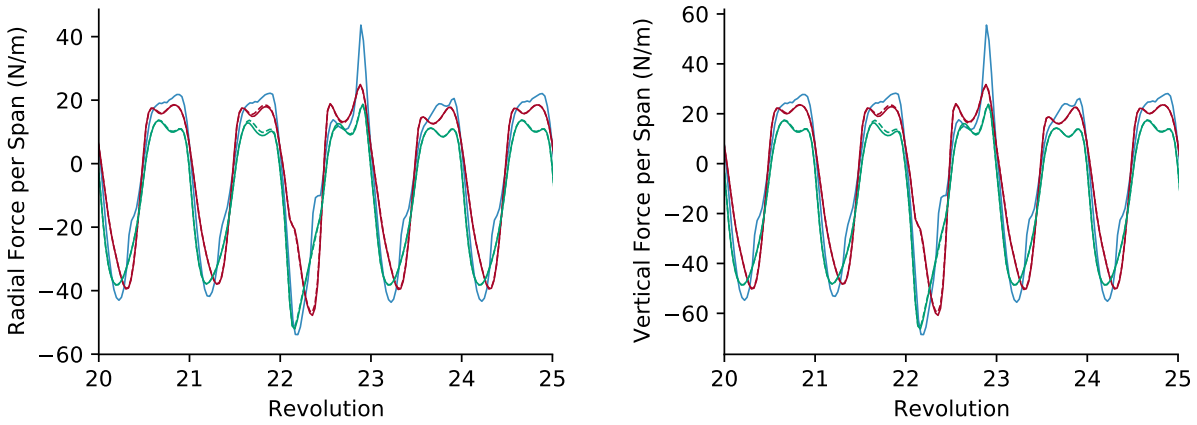

(a) Transient Radial Force Blade 1.

(b) Transient Vertical Force Blade 1.

Fig. 13 Radial and vertical force at 49% height (slice 15). RPI and original 1st order filter methods differ by less than 1%. Plot colors match Fig. 12.

3. Numerical Efficiency

To summarize the numerical efficiency of the RPI method, we run time tests with a i7 3.1GHz processor limited to 1 thread. The CACTUS solver is fortran and is locally compiled per the user instructions. Both AC and DMS are implemented in the Julia language, version 1.5 [29]. The comparison case is the gust case detailed above. CACTUS solves for the entire turbine with 30 vertical discretizations, so for simplicity we multiply the time of the unsteady AC and DMS single slice by 30. For a best case timing scenario, and because dynamic stall is not active at this tip speed ratio, the dynamic stall model was turned off. (Dynamic stall adds about a 1.5x penalty on average but some AC cases can see as much as a 7x penalty). The AC influence coefficient modifications were also turned off and the faster precomputation method used, though vectors of parameters were used in the blade element and residual equations (which has negligible effect on speed). All unsteady simulations were run for 40 revolutions, which gives a real time turbine at 150 rpm 16 seconds to complete the revolutions. The steady case is for 1 revolution, which a real time turbine would complete in 0.4 seconds.

Table 1 Computational speed comparison for a full turbine running for 40 revolutions (16 seconds of simulated time, 0.4 s/rev).

	Steady	1st Order Filter	RPI	3-D Unsteady Vortex
Actuator Cylinder	1.2 s	42 min (1.05 min/rev)	8.35 min (12.53 s/rev)	-
Double Multiple Streamtube	0.06 s	117 s (2.93 s/rev)	11.7 sec (0.29 s/rev)	-
CACTUS	-	-	-	17 hours (25.5 min/rev)

Table 1 summarizes the relative performance. Note that DMS with RPI is the only model able to run faster than real-time for a full 3-D unsteady turbine. The RPI method in this case is only solving for three induced velocities associated with the three blade positions at each timestep. The difference in RPI solution speed is directly proportional to the circumferential discretization. Because this case is discretized by 36, the relative speedup should be 12x (azimuthal discretizations divided by number of blades). This is very nearly realized for the simple DMS method because it uses a 1D superlinear root finder for its residual equation. However, AC requires an n-dimensional root finder due to the intra-turbine coupling. Because the set of equations solved in RPI is non-square for AC (n-blades input minimizing a n-theta residual), a less efficient minimization algorithm (Levenberg-Marquardt [30]) must be used. (When solving AC with the original first order filter, the more efficient trust-region method [31] can be used). This, combined with AC's unchanged overhead associated with the rest of the interrelated analysis makes the speed difference only about 5x faster (azimuthal discretizations divided by number of blades divided by two). A one-to-one comparison puts DMS with RPI at about 5275x faster than CACTUS and enables a new level of system design optimization not previously feasible.

To further close the gap or exceed real-time, we can use larger turbines and parallelization. A larger turbine, such as would be needed for offshore applications, spins much slower, at 5-10 RPM. AC and DMS scale primarily with the number of azimuthal and vertical discretizations and not operating conditions. (This assumes turbulent inflow is not used, otherwise the discretizations may need to be refined.) Therefore, for the same discretization, the simulations will run in about the same amount of time, but the real turbine runs slower. The 40 revolution example above would take the turbine 4-8 minutes instead of 16 seconds to complete. This would give a speedup of 15-30x relative to real-time. This alone does not quite close the gap for unsteady AC, but may give enough margin for a single process computer running DMS with RPI to handle the overhead of real-time 3-D unsteady predictive control. These models also lend themselves well to parallelization due to the uncoupled vertical discretization used by both methods, and particularly for DMS that employs decoupled streamtubes within a slice. Using the same discretizations and number of blades outlined previously, parallelization could give an additional speed increase of up to 30x for AC and 90x for DMS (requiring 30 and 90 parallel processes respectively). In all, these considerations could make AC as much as 28x faster than real-time and DMS as much as 3690x faster than real-time. This could then enable real-time 3-D unsteady predictive control with AC, and more complex processes such as active real-time machine learning with DMS.

VI. Conclusions and Future Work

The motivation of this study was to improve the actuator cylinder (AC) and double multiple streamtube (DMS) models for VAWTs with curved deforming blades. We summarized the linearized 3-D actuator surface derivation as it pertains to a 2-D turbine slice with curved deforming blades. In so doing, we found significant discrepancies due to the original assumptions in both the blade element portions (common to AC and DMS) and intra-turbine aerodynamic coupling (specific to AC). Prior general consensus was that the large (in excess of 50%) discrepancy in forces compared to fully 3-D models was due to these models' 2-D nature. However, we found that by including considerations for curved blades, we could resolve the majority of these discrepancies, reducing the error by a factor of 10. Additionally, we examined deforming blades and reevaluated the method of taking the steady AC and DMS methods into the unsteady domain. We outlined the specific considerations required to accurately model actively deforming curved blades and found a numerically superior rotating point iterative (RPI) solution method. With this method, a 5-10x speedup was realized enabling faster-than-real-time calculations for accurate full turbine unsteady simulations.

The developed speed and accuracy improvements for these 2-D aerodynamic models will enable previously infeasible levels of concurrent system design optimization, essential to the design of floating VAWTs. The next step towards fast and accurate aero-hydro-servo-elastic simulations using these models is to couple and validate aero-elastic simulations. By coupling to a structural code such as OWENS [32] we can explore full aero-elastic turbine design with CACTUS-comparable accuracy, but as much as 5000x faster.

Acknowledgments

This work has been funded by the United States Department of Energy (DOE) Advanced Research Projects Agency – Energy (ARPA-e) under the ATLANTIS program. The views or opinions expressed herein do not necessarily state or reflect those of the United States Government, any agency thereof, or any of their contractors.

References

[1] Templin, R., "Aerodynamic performance theory for the NRC vertical-axis wind turbine," *NASA STI/RECON technical report n*, Vol. 76, 1974. OSTI Report Number(s): N-76-16618; LTR-LA-160.

[2] Wilson, R. E., and Lissaman, P. B., "Applied aerodynamics of wind power machines," *National Science Foundation*, 1974. OSTI Report Number(s): NSF/RA/N-74-113.

[3] Strickland, J., "A performance prediction model for the darrieus turbine," *International symposium on wind energy systems*, 1977, pp. C3–39.

[4] Paraschivoiu, I., "Double-multiple streamtube model for studying vertical-axis wind turbines," *Journal of Propulsion and Power*, Vol. 4, No. 4, 1988, pp. 370–377. https://doi.org/10.2514/3.23076, URL https://doi.org/10.2514/3.23076.

[5] Paraschivoiu, I., and Delclaux, F., "Double multiple streamtube model with recent improvements (for predicting aerodynamic loads and performance of Darrieus vertical axis wind turbines)," *Journal of Energy*, Vol. 7, No. 3, 1983, pp. 250–255. https://doi.org/10.2514/3.48077, URL https://doi.org/10.2514/3.48077.

[6] Ayati, A. A., Steiros, K., Miller, M. A., Duvvuri, S., and Hultmark, M., "A double-multiple streamtube model for vertical axis wind turbines of arbitrary rotor loading," *Wind Energy Science*, Vol. 4, No. 4, 2019, pp. 653–662. https://doi.org/10.5194/wes-4-653-2019, URL https://wes.copernicus.org/articles/4/653/2019/.

[7] Madsen, H., "The Actuator Cylinder - A Flow Model for Vertical Axis Wind Turbines," Thesis, Technical University of Denmark, 01 1982. https://doi.org/10.13140/RG.2.1.2512.3040.

[8] Madsen, H., Larsen, T., Vita, L., and Paulsen, U., "Implementation of the Actuator Cylinder flow model in the HAWC2 code for aeroelastic simulations on Vertical Axis Wind Turbines," *51st AIAA Aerospace Sciences Meeting including the New Horizons Forum and Aerospace Exposition*, 2013. https://doi.org/10.2514/6.2013-913, URL https://arc.aiaa.org/doi/abs/10.2514/6.2013-913.

[9] Cheng, Z., Madsen, H. A., Gao, Z., and Moan, T., "A fully coupled method for numerical modeling and dynamic analysis of floating vertical axis wind turbines," *Renewable Energy*, Vol. 107, 2017, pp. 604 – 619. https://doi.org/https://doi.org/10.1016/j.renene.2017.02.028, URL http://www.sciencedirect.com/science/article/pii/S0960148117301143.

[10] Koppenol, B. S., "Dynamic Analysis of a Floating Vertical Axis Wind Turbine using the Actuator Cylinder Flow Theory - Comparative study on a land-based versus spar vertical axis wind turbine concept and a code-to-code comparison," Thesis, Delft University of Technology, 09 2016. https://doi.org/uuid:24ecd297-323e-4b75-9f76-6b10c337681a.

[11] Ferreira, C. S., Madsen, H. A., Barone, M., Roscher, B., Deglaire, P., and Arduin, I., "Comparison of aerodynamic models for Vertical Axis Wind Turbines," *Journal of Physics: Conference Series*, Vol. 524, 2014, p. 012125. https://doi.org/10.1088/1742-6596/524/1/012125, URL https://doi.org/10.1088%2F1742-6596%2F524%2F1%2F012125.

[12] Ning, A., "Actuator cylinder theory for multiple vertical axis wind turbines," *Wind Energy Science*, Vol. 1, No. 2, 2016, pp. 327–340. https://doi.org/10.5194/wes-1-327-2016, URL https://wes.copernicus.org/articles/1/327/2016/.

[13] Akins, R. E., "Measurements of surface pressures on an operating vertical-axis wind turbine," 1989. URL https://energy.sandia.gov/wp-content/gallery/uploads/SAND-89-7051.pdf, SAND-89-7051.

[14] Ashwill, T. D., "Measured data for the Sandia 34-meter vertical axis wind turbine," 1992. URL https://citeseerx.ist.psu.edu/viewdoc/download?doi=10.1.1.509.1110&rep=rep1&type=pdf, SAND-91-2228.

[15] Sheldahl, R. E., Klimas, P. C., and Feltz, L. V., "Aerodynamic Performance of a 5-Metre-Diameter Darrieus Turbine With Extruded Aluminum NACA-0015 Blades," Tech. Rep. SAND-80-0179, Sandia National Laboratories, 3 1980.

[16] Murray, J., and Barone, M., "The Development of CACTUS, a Wind and Marine Turbine Performance Simulation Code," *49th AIAA Aerospace Sciences Meeting including the New Horizons Forum and Aerospace Exposition*, 2012. https://doi.org/10.2514/6.2011-147, URL https://arc.aiaa.org/doi/abs/10.2514/6.2011-147.

[17] Tavernier, D. D., Sakib, M., Griffith, T., Pirrung, G., Paulsen, U., Madsen, H., Keijer, W., and Ferreira, C., "Comparison of 3D aerodynamic models for vertical-axis wind turbines: H-rotor and Φ-rotor," *Journal of Physics: Conference Series*, Vol. 1618, 2020, p. 052041. https://doi.org/10.1088/1742-6596/1618/5/052041, URL https://doi.org/10.1088%2F1742-6596%2F1618%2F5%2F052041.

[18] Cheng, Z., Madsen, H. A., Gao, Z., and Moan, T., "Aerodynamic Modeling of Floating Vertical Axis Wind Turbines Using the Actuator Cylinder Flow Method," *Energy Procedia*, Vol. 94, 2016, pp. 531 – 543. https://doi.org/https://doi.org/10.1016/j.egypro.2016.09.232, URL http://www.sciencedirect.com/science/article/pii/S1876610216309195, 13th Deep Sea Offshore Wind R&D Conference, EERA DeepWind'2016.

[19] Wang, K., Hansen, M., and Moan, T., "Model improvements for evaluating the effect of tower tilting on the aerodynamics of a vertical axis wind turbine," *Wind Energy*, Vol. 18, 2014, pp. 91–110. https://doi.org/10.1002/we.1685.

[20] Leroy, V., "Unsteady aerodynamic modelling for seakeeping analysis of Floating Offshore Wind Turbines," Theses, École centrale de Nantes, Dec. 2018. URL https://tel.archives-ouvertes.fr/tel-02090543.

[21] Glauert, H., *The Elements of Aerofoil and Airscrew Theory*, Cambridge Science Classics, Cambridge University Press, 1983. https://doi.org/10.1017/CBO9780511574481.

[22] Larsen, T., and Aagaard Madsen, H., "On the way to reliable aeroelastic load simulation on VAWT's," 2013. URL http://www.ewea.org/annual2013/, european Wind Energy Conference ; Exhibition 2013, EWEA 2013 ; Conference date: 04-02-2013 Through 07-02-2013.

[23] Sørensen, N., Aa, H., and Madsen, H., "Modelling of transient wind turbine loads during pitch motion," *European Wind Energy Conference and Exhibition 2006, EWEC 2006*, Vol. 1, 2006.

[24] Sheldahl, R. E., and Blackwell, B. F., "Free-Air Performance Tests of a 5-Metre-Diameter Darrieus Turbine," Tech. Rep. SAND-77-1063, Sandia National Laboratories, 12 1977.

[25] Klimas, P. C., and Worstell, M. H., "Effects of blade preset pitch/offset on curved-blade Darrieus vertical axis wind turbine performance," 1981. SAND-81-1762.

[26] Tarzanin, F., "Prediction of control loads due to blade stall," *Journal of the American Helicopter Society*, Vol. 17, No. 2, 1972, pp. 33–46. https://doi.org/https://doi.org/10.4050/JAHS.17.33.

[27] Madsen, H., "Application of Actuator Surface Theory on Wind Turbines," Technical University of Denmark, 1988.

[28] Taylor, G. I., "The Spectrum of Turbulence," *Proceedings of the Royal Society A: Mathematical, Physical and Engineering Sciences*, Vol. 164, No. 919, 1938, pp. 476–490. https://doi.org/10.1098/rspa.1938.0032, URL https://royalsocietypublishing.org/doi/abs/10.1098/rspa.1938.0032.

[29] Bezanson, J., Edelman, A., Karpinski, S., and Shah, V. B., "Julia: A fresh approach to numerical computing," *SIAM review*, Vol. 59, No. 1, 2017, pp. 65–98. URL https://doi.org/10.1137/141000671.

[30] Moré, J. J., "The Levenberg-Marquardt algorithm: implementation and theory," *Numerical analysis*, Springer, 1978, pp. 105–116. URL https://www.osti.gov/servlets/purl/7256021/.

[31] Byrd, R. H., Schnabel, R. B., and Shultz, G. A., "A trust region algorithm for nonlinearly constrained optimization," *SIAM Journal on Numerical Analysis*, Vol. 24, No. 5, 1987, pp. 1152–1170. https://doi.org/10.1137/0724076.

[32] Owens, B. C., "Theoretical Developments and Practical Aspects of Dynamic Systems in Wind Energy Applications," Ph.D. thesis, Texas A & M University, 2013. URL http://hdl.handle.net/1969.1/151813.